JOURNAL OF SOLID STATE CHEMISTRY 91, 250–263 (1991)

Topological Relation between the LaIrSi- and the EuNiGe-Type Structures in Ternary Phases *M*PdSi (*M* = Ca, Eu, Sr, Ba)

JÜRGEN EVERS, GILBERT OEHLINGER, KURT POLBORN, AND BERND SENDLINGER

Institut für Anorganische Chemie der Universität München, Meiserstrasse 1, D-8000 München 2 (FRG)

Received August 17, 1990; in revised form November 5, 1990

The LaIrSi-type structure has been established for SrPdSi ($cP12$, $P2_13$, a = 650.0(1) pm, R = 4.40%) by a single crystal investigation and for EuPdSi (a = 641.9(1) pm) and BaPdSi (a = 666.2(1) pm) by Guinier powder experiments in Rietveld technique. In the LaIrSi-type structure a three-dimensional net is built up in which each transition metal atom has three Si neighbors (and vice versa). This net is a slightly distorted version of the ideal (10,3)a-net and projects as 4.8^2-net. For CaPdSi ($mP12$, $P2_1/n$, a = 588.2(1), b = 575.3(1), c = 734.7(1) pm, β = 109.63(1)°, R = 2.05%) the EuNiGe-type structure has been derived by a single crystal investigation. Again, each transition metal atom has three Si neighbors (and vice versa), but now layers of distorted 4.8^2-nets are formed. This net is reminiscent of the (10,3)d-net and shows a topological relation to the (10,3)a-net found in the LaIrSi-type structure. The nets differ in the chirality of their constituent screws of three-connected atoms. Due to the denser packing of the EuNiGe-type structure in comparison to the LaIrSi-type structure a high pressure transformation of the second to the first is favored.

Introduction

Silicides form an exciting class of solids in which directed bonds extend indefinetely in one, two, or three dimensions forming chains, layers, or nets, respectively. In the ternary phases *M*PtSi (*M* = Ca, Eu, Sr, Ba) (*1*) with the LaIrSi-type structure (*2*) the Pt and the Si atoms build up the cubic three-dimensional three-connected (3D3C) net in an ordered arrangement. This net is a slightly distorted arrangement of the ideal (10,3)a-net derived from a topological point of view by Wells (*3–9*). The (10,3)a-net is unique: it contains eight three-connected points in a cubic cell forming 10-membered rings with equidistant bonds ($\sqrt{2} \cdot a_l/4$, a_l = lattice parameter) and equal bond angles of 120°. The three-connected groups are coplanar, but 70.52° turned from another. The (10,3)a-net represents the three-connected analogue of the four-connected diamond net. In the cubic diamond net eight four-connected points form 6-membered rings with equidistant links ($\sqrt{3} \cdot a_l/4$) and equal bond angles of 109.47°. Due to the denser packing of the four-connected net (space filling 34.01%), it is stable for group IV elements (C II, Si I, Ge I, Sn II), for the zinc-blende and wurtzite phases (e.g., AlP, ZnS, CuCl) and for the NaTl-type structure Zintl phases. However, in the three-connected net space filling is only 18.51%. As a result, it has not been observed for group V elements, but only for Zintl phases $SrSi_2I$ (normal pressure (NP) phase) (*10–12*) and

0022-4596/91 $3.00

$BaSi_2$ III (high pressure (HP) phase) (*13, 14*) with the $SrSi_2$-type structure (space group $P4_332$ or $P4_132$) (*10*). Here the divalent *M* atoms Sr or Ba fill the large cavities of the net.

The 3D3C net in the $SrSi_2$-type structure deviates slightly from the ideal (10,3)a-net (*15*). It consists of equidistant bonds and equal bond angles. But at 118°, the bond angles are smaller than the ideal value of 120°. The three-connected groups are slightly puckered and turned 74° from another. However, in the ternary phases with the LaIrSi-type structure (*2*) there are still equal bond distances, but with two slightly different bond angles. Interestingly, in the ternary phases *M*PtSi this structure has a stability range for metals with radii from r_{Ca} = 197.4 to r_{Ba} = 224.3 pm in contrast to binary MSi_2 compounds which exist with the $SrSi_2$-type structure only from r_{Sr} = 215.1 to r_{Ba} = 224.3 pm.

Nevertheless, the 3D3C net in CaPtSi I (*1*), with remarkably short Pt–Si distances of 229.7(5) pm, can be transformed into a denser packed HP phase in a belt apparatus at 4 GPa and 800°C. Since isolation of single crystals of the HP phase CaPtSi II failed up to now, structural investigations have been performed by Guinier technique on microcrystalline powders. Automatic indexing (*16*) of the Guinier diffractogram lead to a monoclinic unit cell with four formula units.

Due to the low symmetry of the HP phase CaPtSi II, its crystal structure could not be solved using powders and it was decided to prepare single crystals at NP by slow melt-cooling of a system which is chemically strong related to, but denser packed than, CaPtSi I. The metallic radius of platinum for CN 12 (r_{Pt} = 138.7 pm) is only slightly higher than that of palladium (r_{Pd} = 137.6 pm) (*17*). Therefore, it is evident that a pressure of about 1 GPa is sufficient to squeeze Pt to the size of Pd at NP. Thus, it is expected that the study of the ternary phases *M*PdSi (*M* = Ca, Eu, Sr, Ba) at NP leads to information about the structural behavior of the MPtSi phases at HP.

TABLE I

METALLIC IMPURITIES IN Ca, Eu, Sr, Ba, Pd DETERMINED BY ICP-ATOMIC ABSORPTION SPECTRAL ANALYSIS (*21*)

Impurity (wt ppm)	Ca	Eu	Sr	Ba	Pd
Mg	32	20	397	17	154
Ca		16	153	14	126
Sr	147	13		4	4
Ba	21	6	675		2
Al	5	9	31		106
Si	21	5	101	5	93
Ti		67	1	1	4
Cr	2		3	1	20
Mn	17	23	1	28	2
Fe	4	8	9	2	254
Ni	2		3	1	265
Cu	3		5	1	43
Zn	9		25	5	63
Sn	6		4	1	11
Mo	3	19	8	1	12
Pb	12	8	22	6	980
Σ	284	217	1438	85	2139
Purity (wt%)	99.97	99.98	99.86	99.99	99.79

In this paper we report on synthesis and characterization of the MPdSi phases. Single crystal investigations on a four-circle diffractometer were performed on CaPdSi and SrPdSi. In addition, powders of CaPdSi, EuPdSi, SrPdSi, and BaPdSi were studied on a computer-controlled Guinier diffractometer. In this case structural information was derived by the Rietveld technique (*18*). The divalency of europium in EuPdSi was checked by magnetic measurements on a Faraday balance.

Experimental

The title compounds were prepared from the elements: electronic grade silicon (Wacker, FRG), palladium powder (De-

TABLE II

CRYSTALLOGRAPHIC DATA FOR CaPdSi

Structure Type			EuNiGe		
Crystal System			Monoclinic		
Space Group			$P2_1/n$		
Lattice Parameters (pm)[a]			a = 588.2(1) b = 575.3(1) c = 734.7(1)		
(°)			β = 109.63(1)		
Density (g/cm^3)					
Experimental			4.64		
Calculated			4.69		
Formula/unit-cell			4		
Positional and thermal parameters		x	y	z	U_{eq}(Å^2)
4 Ca		0.3185(3)	0.1281(3)	0.1151(2)	0.0084(4)
4 Pd	in 4(e)	0.9223(1)	0.1098(1)	0.30997(8)	0.0075(1)
4 Si		0.3271(4)	0.1194(4)	0.5450(3)	0.0084(5)

[a] ESD's in parentheses

gussa, FRG), and ultra-high vacuum-distilled metals (*19, 20*) calcium, europium, strontium, and barium. By ICP-atomic absorption spectral analysis (*21*) the five metallic materials were characterized trace analytically. The results are summarized in Table I. Synthesis of the MPdSi phases was performed by quasi crucible-free melting of the above elements in an inductively heated water-cooled copper boat under purified argon. The copper boat could be transferred into the glovebox in which argon is continuously recirculated and purified. In a first melting experiment an excess of about 5% of the divalent metal (Ca, Eu, Sr, Ba, respectively) was used. By weighing the regulus (approximately 1000 mg mass) the evaporation loss of the divalent metal was determined. After adding calculated amounts of Pd and Si in a subsequent second melting experiment nearly stoichiometric samples were prepared. For X-ray powder experiments capillaries (0.3 mm diameter) were filled in the glovebox, sealed, and investigated without further annealing. Single crystals of CaPdSi and SrPdSi were prepared in a high vacuum tight furnace under argon by cooling the melt at a rate of 1°/min in corundum crucibles and then also sealed into capillaries.

On a computer-controlled Guinier diffractometer (G644, Huber-Diffraktionstechnik, Mo$K\alpha$1 radiation, quartz-monochromator), calibrated with electronic grade germanium, Guinier diffractograms of CaPdSi, EuPdSi, SrPdSi, and BaPdSi were obtained. For CaPdSi, 1500 data points were collected in the 2θ range between 6 and 36° and for EuPdSi, SrPdSi, and BaPdSi 2000 data points between 8 and 48°, all with an increment of 0.02° (2θ) and a counting rate of 100 sec per increment, were collected. In this manner the diffractograms showed a very low signal-to-noise relation. The background was linearized by subtracting a background file from the original data. After application of an absorption correction for cylindrical samples (*22*) the data set was normalized to an intensity maximum of 500 counts per second for the strongest reflection and to 25 cps for the linear background. The Gui-

TABLE III

CRYSTALLOGRAPHIC DATA FOR SrPdSi
(For Reasons of Comparison Crystallographic Data for $SrSi_2$ I Are Also Given (*12*))

	SrPdSi			$SrSi_2$ I	
Structure type	LaIrSi			$SrSi_2$	
Crystal system	Cubic			Cubic	
Space group	$P2_13$			$P4_332$ or $P4_132$	
Lattice parameter a (pm)[a]	650.0(1)			653.5(3)	
Density (g/cm^3)					
Experimental	5.32			3.40	
Calculated	5.29			3.42	
Formula/unit-cell	4			4	
Positional and thermal parameters[b]	x	U_{eq}(Å^2)		x	U_{eq}(Å^2)
Sr:	0.1307(1)	0.0185(10)	Sr:	0.125	0.0108(2)
Pd:	0.4103(2)	0.0179(8)	Si:	0.42248(9)	0.0090(3)
Si:	0.8372(8)	0.0184(33)	Si:	0.82752(9)	0.0090(3)

[a] ESDs in parentheses.
[b] SrPdSi: 4 Sr, 4 Pd, 4 Si in 4(a), P 2_13. $SrSi_2$: 4 Sr in 4(a), 8 Si in 8(c), P 4_332.

nier diffractograms of CaPdSi, EuPdSi, SrPdSi, and BaPdSi were indexed automatically by the DICVOL method (*16*) and then analyzed by the Rietveld technique for structural data (*18*).

The single crystals of CaPdSi (0.13 × 0.07 × 0.03 mm^3) and SrPdSi (0.06 × 0.05 × 0.04 mm^3) do not show well-developed faces. For CaPdSi, preliminary Weißenberg photographs indicated the Laue symmetry $2/m$ with systematic absences $h0l$: $h + l \neq 2n$ and $0k0$: $k \neq 2n$. This leads to the monoclinic space group $P2_1/n$ for CaPdSi. From Weißenberg photographs it was also derived that SrPdSi and CaPtSi I (*1*) (LaIrSi-type structure) (*2*) are isotypic and belong to the cubic space group $P2_13$ (Laue symmetry $m\bar{3}$, systematic absences $h00$: $h \neq 2n$).

For single crystal structure analysis, data were collected on a Enraf-Nonius-CAD4 diffractometer in the 2θ-range (ω-scan mode) 4–50° for CaPdSi and 4–46° for SrPdSi with filtered Mo$K\alpha$ radiation. In the Miller index range $\pm h$, $\pm k$, $+l$, 917 reflections were measured for CaPdSi and in the range $+h$, $+k$, $+l$, 253 reflections were measured for SrPdSi. After absorption correction (μ = 101 and 381 cm^{-1} for CaPdSi and SrPdSi, respectively) there remained unique sets of 356 observed reflections with $I > 2\sigma(I)$ (R_{int} = 2.8%) for CaPdSi and of 76 reflections (R_{int} = 6.8%) for SrPdSi. All structural calculations were performed with the SHELXTL-program system (*23*). CaPdSi (structure solved by direct methods and refined by Fourier techniques (R = 2.05%, R_w = 2.63%)) is isotypic to EuNiGe (*24*). For SrPdSi (R = 4.40%, R_w = 5.20%), starting positional parameters were those of CaPtSi with the LaIrSi-type structure (*1*).

The magnetic susceptibility of EuPdSi was measured in Faraday technique on a Cahn microbalance. During the measurements the magnetic field was varied between 1.5 and 5.0 kOe and the temperature between 77 and 528 K.

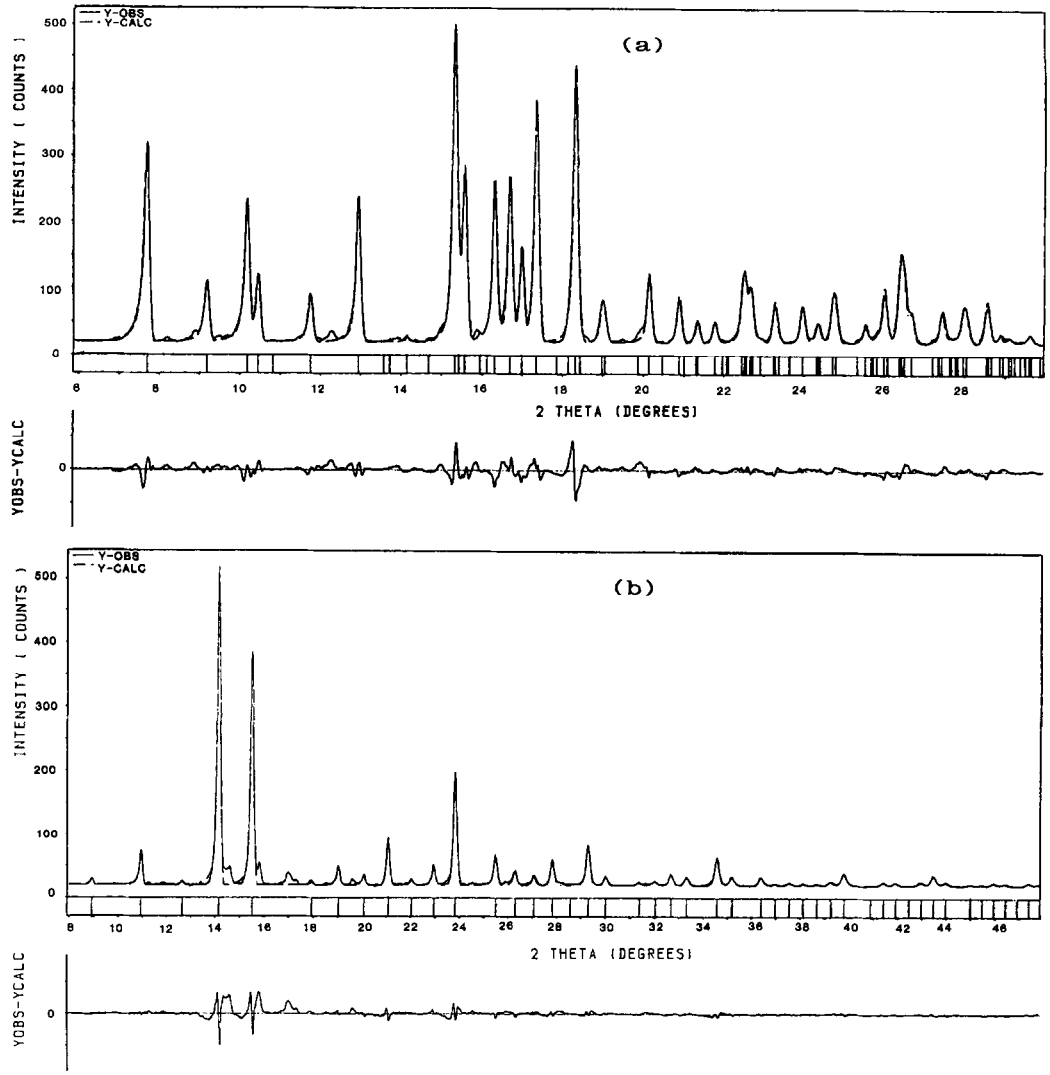

FIG. 1. Rietveld refinement patterns (*18*) for *M*PdSi (*M* = Ca, Eu, Sr, Ba): increment 0.02° (2Θ), counting rate pro increment 100 sec. The observed Guinier diffractogram is indicated by a solid line, the calculated one by a broken line overlaying the first. 2Θ-positions for possible reflections are marked by vertical lines. The lower curve shows the difference plot between the observed and the calculated diffractogram. (a) CaPdSi, 2Θ range: 6–36°; R_p = 7.26%. (b) EuPdSi, 2Θ range: 8–48°; R_p = 7.24%. (c) SrPdSi, 2Θ range: 8–48°; R_p = 8.74%. (d) BaPdSi, 2Θ range: 8–48°; R_p = 3.69%.

Results

The Guinier diffractograms of EuPdSi, SrPdSi, and BaPdSi indicated isotypic compounds with the LaIrSi-type structure (*2*). They were indexed as cubic phases with reliability indices F_{N20} (*25*) of 70, 48, and 48, respectively. These values are remarkable higher than the minimum value of 20 required for correct indexing. Rietveld analy-

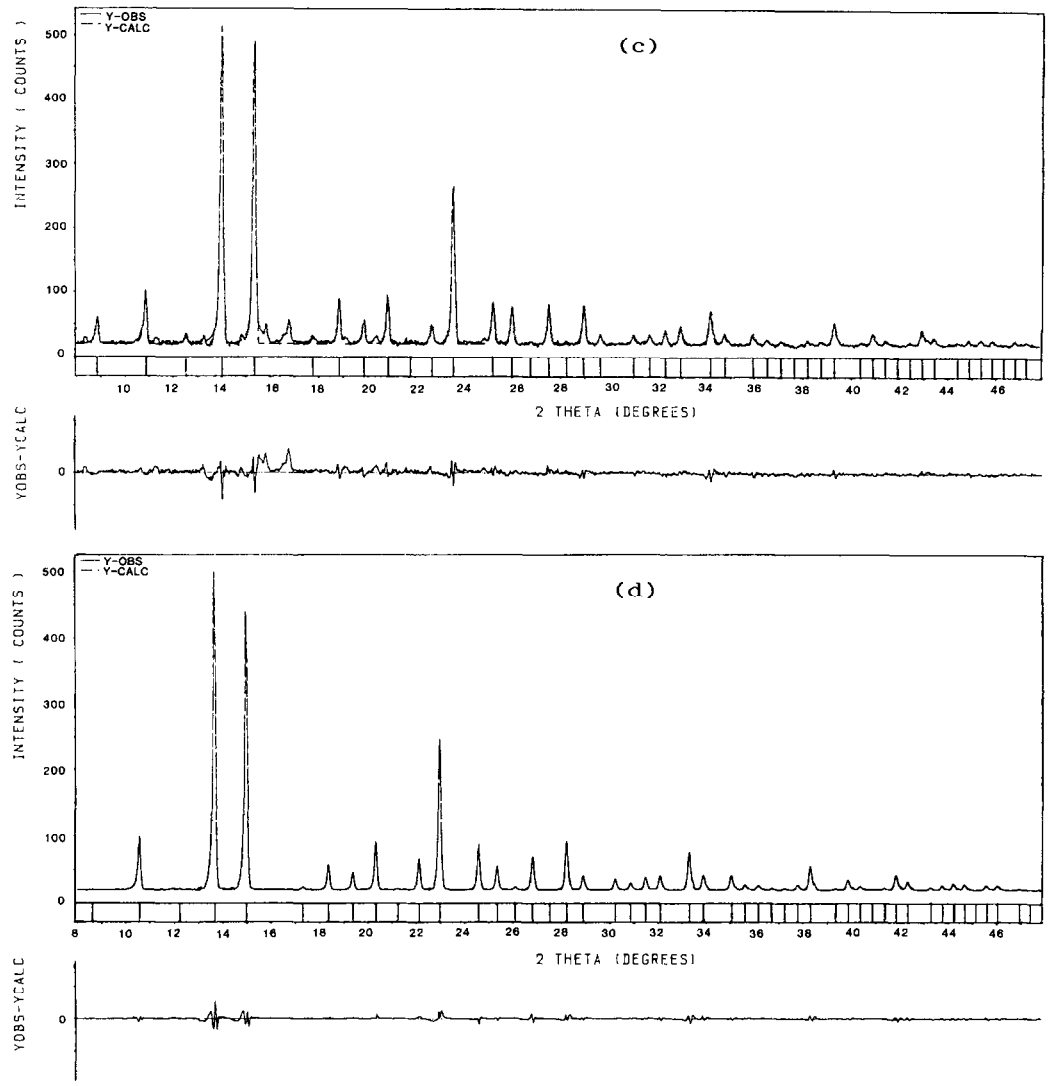

FIG. 1.—*Continued*

sis led to lattice parameters 641.9(1), 650.0(0), and 666.2(1) pm for EuPdSi, SrPdSi, and BaPdSi, respectively. The Guinier diffractogram of CaPdSi is quite different from that of the phases crystallizing in the LaIrSi-type structure. Strong analogies were found to the quite weaker diffractogram of HP-CaPtSi II. Automatic indexing led to monoclinic cells for CaPdSi and CaPtSi II with reliability indices F_{N20} of 65 and 10, respectively.

The crystallographic data determined by the single crystal investigations on CaPdSi and SrPdSi are presented in Tables II and III. For reasons of comparison, crystallographic data for $SrSi_2$ I derived by a single crystal investigation on a four-circle diffractometer (318 independent reflections, R_w =

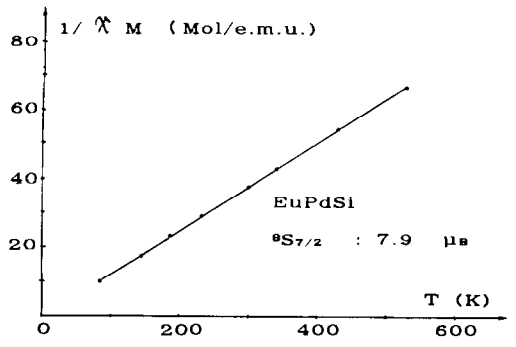

FIG. 2. Reciprocal molar susceptibility of EuPdSi as function of the absolute temperature. From the slope of the Curie–Weiss line a magnetic moment of 7.9 μ_B/Eu atom is calculated.

2.28%) (*12*) are also given in Table III. Rietveld refinement patterns (*18*) are presented in Figs. 1a–1d for CaPdSi, EuPdSi, SrPdSi, and BaPdSi.

The reciprocal molar magnetic susceptibility of EuPdSi (not corrected for a diamagnetic contribution) is plotted against the absolute temperature in Fig. 2. From the slope of the Curie–Weiss line a magnetic moment of 7.9 μ_B/Eu atom is calculated. Within the limitations of error this value agrees with the $^8S_{7/2}$ ground state of Eu(II) for which 7.94 μ_B/Eu atom is expected. Therefore it is concluded that in EuPdSi between 77 and 528 K europium is divalent.

Discussion

As mentioned above, the ternary compounds *M*PdSi (*M* = Ca, Eu, Sr, Ba) crystallize in the monoclinic EuNiGe- (*24*) and in the cubic LaIrSi-type structure (*2*). The transition metal atoms *T* (=Pd) and the semimetal atoms *S* (=Si) form three-connected nets which are topologically related to (10,3)-nets, derived by Wells (*3–9*). The 3D3C net of the LaIrSi-type structure is a distortion of the cubic (10,3)a-net and the three-connected net of the EuNiGe-type structure is obtained from the orthorhombic (10,3)d-net after shifting *x* and *z* parameters by $\approx \pm 1/16$ and lowering the symmetry to the monoclinic system.

Among the 3D3C nets the (10,3)a-net in its ideal arrangement (equidistant bonds with equal bond angles of 120°) is described in space group $I4_132$ with eight points in position 8(b) ($x = 3/8$). Due to its low degree of space filling (18.51%), the (10,3)a-net is only found in binary and ternary compounds with additional metal atoms filling the cavities and stabilizing the structure. In binary compounds with the $SrSi_2$-type structure ($SrSi_2$ I and $BaSi_2$ III) the *M*-atoms are found in position 4(a) and the Si atoms in position 8(c) of space group $P4_332$ or $P4_132$. In the ternary compounds with the LaIrSi-type structure, e.g., SrPdSi, 4 Sr, 4 Pd, and 4 Si occupy position 4(a) of space group $P2_13$. Figure 3a shows a projection of four unit cells of SrPdSi (without Sr atoms) down [001] for the ideal positional parameter $x_T = 3/8$ and $x_S = 7/8$ (heights *z* are presented as multiples of 1/8). In this case the 3D3C net is built up by four-fold screws of *T* and *S* atoms with uniform chirality. Within such a screw there are two bonds. The third bond is formed by connection with one adjacent screw at the same height *z*. The ideal (10,3)a-net projects two-dimensionally as semiregular 4.8^2-net: here each *T* (or *S*) atom is connected to one square and two octagons (Fig. 3a). However, in SrPdSi the 3D3C net shows a deviation from the ideal net due to shifting of the positional parameter. For $x_{Pd} = 0.4103$ and $x_{Si} = 0.8372$ (Table III) the slightly distorted screws are rotated 32° against each other (Fig. 3b). As a consequence, space filling is increased from 18.51% for the ideal (10,3)a-net to 19.72% for the distorted arrangement in SrPdSi.

The shift of the positional parameters in SrPdSi in relation to $SrSi_2$ I (Table III) results in a shift of 8 and 7 pm for the three-connected atoms in the net. This leads to a

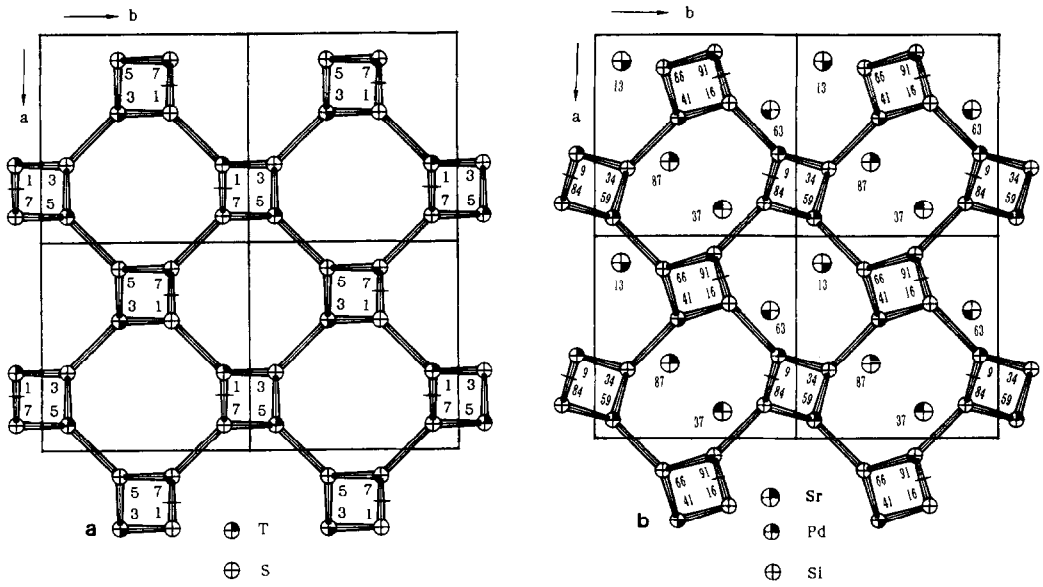

FIG. 3a. Projection of four unit cells of the ideal (10,3)a-net down [001]. Heights z are presented as multiples of 1/8. Each T atom has three S neighbors (and vice versa) and connections to adjacent screws are formed by T–S bonds at equal heights z.

FIG. 3b. Projection of four unit cells of the distorted (10,3)a-net down [001] in SrPdSi (LaIrSi-type structure). Heights z are presented as multiples of 1/100. Four Sr atoms fill the two large cavities within one unit cell. Each Pd atom has three Si neighbors (and vice versa) and connections between adjacent screws are formed by Pd–Si bonds at slightly different heights z.

decrease of the bond distance in the net of the ternary phase which is more than two times stronger than the decrease of the corresponding lattice parameters. In the system $SrSi_2$ I/SrPdSi there is a decrease in bond distance of 1.9% (239.2/234.7 pm, Table IV) and a decrease in the lattice parameters of only 0.5% (653.5/650.0 pm, Table III). This holds also for the system $BaSi_2$ III/BaPdSi. The analogous data are: 2.3% decrease in bond distance (244.7/239.2 pm, Table V) and only 0.8% decrease in lattice parameters (671.5 (*13*, *14*)/666.2 pm).

This behavior is also reflected in the variation of the positional parameters x_M, x_{Pd}, and x_{Si}, which were derived by the Rietveld technique for EuPdSi and BaPdSi. Interestingly, they show for these three compounds a characteristic variation as a function of increasing metallic radius r_M (M = Eu, Sr, Ba). The x_M and x_{Si} parameters increase and the x_{Pd} parameter decreases. By this way the ratio of the bond distances M–M/Pd–Si for the ternary phases remains nearly constant at 1.70, 1.70, and 1.71, for EuPdSi, SrPdSi, and BaPdSi, respectively (*18*) (Table V). For $SrSi_2$ I and $BaSi_2$ III the analogous ratios M–M/Si–Si are lower (1.67 and 1.68, respectively, Table V) (*12*), since here the longer bond distance is in the denominator. It seems that the increase of bond strength in the 3D3C net of the ternary phase is one reason for its greater stability range in comparison to the binary phase. At NP the $SrSi_2$ type structure is stable only for $SrSi_2$ I and at HP for $BaSi_2$ III. For MTSi phases (M = Ca, Eu, Sr, Ba; T = Pd, Pt) the LaIrSi-type structure is stable for four

TABLE IV

NUMBER OF NEIGHBORS, BOND DISTANCES (pm), AND BOND ANGLES (°) FOR SrPdSi AND $SrSi_2$ I [12]

	SrPdSi	$SrSi_2$ I
Sr neighbors:[a]		
	–1 Pd 314.8(3)	–6 Si 325.3(3)
	–1 Si 330.4(3)	–2 Si 336.7(3)
	–3 Pd 332.0(3)	–6 Si 382.7(3)
	–3 Si 333.1(3)	–6 Sr 400.2(2)
	–3 Si 371.6(3)	
	–3 Pd 380.6(3)	
	–6 Sr 398.2(4)	
Si neighbors:		
	–3 Pd 234.7(4)	–3 Si 239.2(1)
	–1 Sr 330.4(3)	–3 Sr 325.5(3)
	–3 Sr 333.1(3)	–1 Sr 336.7(3)
	–3 Sr 371.6(3)	–3 Sr 382.7(3)
Pd neighbors:		
	–3 Si 234.7(4)	
	–1 Sr 314.8(3)	
	–3 Sr 332.0(3)	
	–3 Sr 380.6(3)	
Bond angles:		
	$Pd^{Si}Pd$ 118.5(1)	$Si^{Si}Si$ 117.8(1)
	$Si^{Pd}Si$ 118.8(1)	

[a] ESDs in parentheses.

Pt compounds (CaPtSi, EuPtSi, SrPtSi, BaPtSi) (*1*) and three Pd compounds (EuPdSi, SrPdSi, BaPdSi), but not for CaPdSi (*19*). For the last compound, a Pd–Si bond distance which must be smaller than the Pt–Si distance in CaPtSi I (229.7(5) pm (*1*)) is expected. Apparently, such a bond distance is too small for the 3D3C net built up by Pd and Si atoms with Ca atoms filling the cavities. Therefore, a structural change takes place: the Pt compound is related to the (10,3)a-net, the Pd compound is reminiscent of the (10,3)d-net derived by Wells (*8*).

In the (10,3)a-net screws of uniform chirality build up the 3D3C net (Figs. 3a, 3b). On the other hand, in the (10,3)d-net the screw chirality differs characteristically: here each screw is connected to four adjacent screws with opposite chirality. According to Wells, the most symmetrical configuration of the (10,3)d-net is found in the space group *Pnna* (*8*) (position 8(e) (7/8, 1/8, 5/8) (Table VI)). This net is less symmetric than the (10,3)a one. Bond angles (144.7, 120, and 90°) and also bond distances differ remarkably. Two bond distances within the screws are $\sqrt{2} \cdot a_1/4$, but the bond distance between the screws is longer ($\sqrt{3} \cdot a_1/4$). This results in a trend for denser packing of about 4.5% of the (10,3)d-net in comparison to the (10,3)a one. Therefore a high pressure dimorphy between the (10,3)a- and the (10,3)d-net is favored.

However, in space group *Pnna* no ordering of *T* and *S* atoms is possible, since position 8(e) is statistically occupied. Lowering the symmetry to the monoclinic space group $P2_1/n$ for *T* atoms in position 4(e) at (7/8, 1/8, 5/8) (and for *S* atoms at (3/8, 1/8, 5/8)) ordering is possible. Also this net projects two-dimensionally as a 4.8^2-net (Fig. 4a).

TABLE V

AVERAGE BOND DISTANCES AND THEIR RATIO FOR EuPdSi, SrPdSi, BaPdSi, $SrSi_2$ I (12), AND $BaSi_2$ III (12)

	Bond distance			Ratio	
	M–*M*	Pd–Si	Si–Si	*M*–*M*/Pd–Si	*M*–*M*/Si–Si
EuPdSi	393.2(3)	231.8(5)		1.70	
SrPdSi	398.2(3)	234.7(4)		1.70	
BaPdSi	408.5(4)	239.3(5)		1.71	
$SrSi_2$ I	400.2(2)		239.2(1)		1.67
$BaSi_2$ III	411.2(2)		244.7(1)		1.68

TABLE VI

BOND ANGLES, BOND DISTANCES, AND SPACE FILLING FOR (10,3)-NETS

	(10,3)a-net	(10,3)d-net
Space group	$I4_132$	*Pnna*[a]
Position	8(b)	8(e)
	(3/8, 3/8, 3/8)	(7/8, 1/8, 3/8)
Bond angles (°)	120 (3×)	144.7, 120, 90
Bond distances as function of lattice parameter a_1	$\sqrt{2} \cdot a_1/4$ (3×)	$\sqrt{2} \cdot a_1/4$ (2×), $\sqrt{3} \cdot a_1/4$ (1×)
Space filling (%)	18.51	22.99[b]

[a] With constraints $a = b = c$.
[b] Calculated for average bond distance.

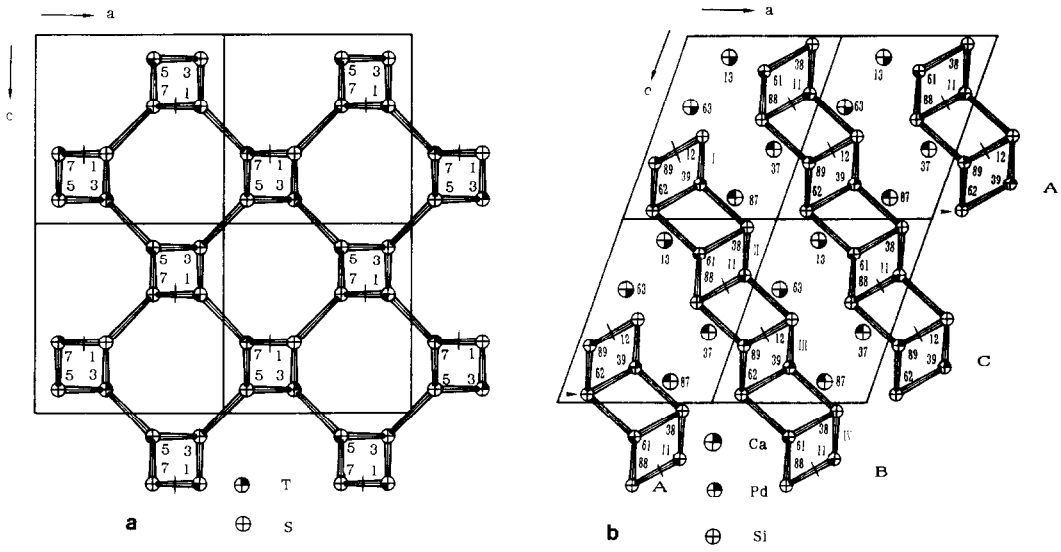

FIG. 4a. Projection of four unit cells of the (10,3)d-net down [010]. Heights y are presented as multiples of 1/8. Each T atom has two S and one T neighbor (and vice versa). Connections between adjacent screws are formed by either S–S or T–T bonds at different heights y. (Additional contraints for lattice parameters: $a = b = c$)

FIG. 4b. Projection of four unit cells of the distorted (10,3)d-net down [010] in CaPdSi. Heights y are presented as multiples of 1/100. In comparison to Fig. 4a the x and z positional parameter of the T and S atoms are shifted by $\approx \pm 1/16$ and the symmetry is lowered to the monoclinic system. The three-connected Pd and Si atoms form layers of distorted 4.8^2 nets parallel to $(10\bar{1})$ in the sequence A,B,C,A . . . separated by layers of Ca atoms. Two Si atoms which achieve identity after three layers are marked with an arrow. The screws which built up the 4.8^2 motif of Fig. 5 are numbered from I to IV.

TABLE VII

FRACTIONAL COORDINATES FOR THE (10,3)D-NET AND ITS DISTORTED ARRANGEMENT IN CaPdSi

	(10,3)d-net	Distorted arrangement
4 Pd[a]	(7/8, 1/8, 3/8)	(15/16, 1/8, 5/16) (0.9223, 0.1098, 0.3100)[b]
4 Si	(3/8, 1/8, 5/8)	(5/16, 1/8, 9/16) (0.3271, 0.1194, 0.5450)[b]

[a] Position 4(e), $P2_1/n$

[b] Positional parameters of Pd and Si in Table II.

Unfortunately, T (S) atoms cannot be connected to 3 S (T) atoms in this arrangement. Since the connection between the screws is built up by either T–T or S–S bonds: each T atom has two S and one T neighbor (and vice versa). In Fig. 4a a projection of the (10,3)d-net (with constraints for lattice parameters: $a = b = c$, $\alpha = \beta = \gamma = 90°$) down [010] is shown (heights y are presented as multiples of 1/8). It seems that for a ternary phase MTSi (T = Pd, Pt), a structure with a (10,3)d arrangement is less stable than its distorted version.

Rotating the screws against each other by shifting the x- and the z-positional parameters of the S and T atoms by $\approx\pm 1/16$ the interconnection of the screws is changed (Table VII) and the three-dimensional (10,3)d-net is converted into a layer structure. This leads to two advantages: first, bonding of the T atoms to three S atoms (and vice versa) takes place, and second, connection between the screws is performed at nearly the same height y. The three-connected T and S atoms form now distorted 4.8^2-layers parallel $(10\bar{1})$ in the sequence A,B,A . . . Applying constraints for the lattice parameters ($a = b = c$) two shorter bonds ($3a_1/8$) and one 20% longer bond ($\sqrt{13} \cdot a_1/8$) are obtained within a layer.

Due to the low degree of space filling in the (10,3)-nets, four M atoms at (1/8, 1/8, 1/8) (position 4(a), space group $P4_332$; Table III) fill the cavities of the (10,3)a-net. Since there are two cavities within one unit-cell two M atoms are placed in each (Fig. 3b). However, for the (10,3)d-net analogous positions for the four M atoms are at (3/8, 1/8, 1/8) (position 4(e), $P2_1/n$). Unfortunately, with constraints for lattice parameters ($a = b = c$, $\alpha = \beta = \gamma = 90°$) there will appear very short M–Pd and M–Si bonds. Therefore the positional parameter x of the Ca atoms has to be shifted by $\approx\pm 1/16$ from (3/8, 1/8, 1/8) to (5/16, 1/8, 1/8).

Lowering the symmetry in CaPdSi from orthorhombic to monoclinic (different length for the lattice parameters a and c, ($c/a \approx 1.25$); angle $\beta \approx 110°$, Table II), the distances Ca–Ca, Ca–Pd and Ca–Si on one side and Pd–Si on the other achieve common ranges (Table VIII). In addition, the

TABLE VIII

NUMBER OF NEIGHBORS, BOND DISTANCES (pm), AND BOND ANGLES (°) FOR CaPdSi

Ca neighbors:		
	–1 Pd 293.1(1)	–1 Pd 326.5(1)
	–1 Si 301.9(2)	–1 Pd 331.0(1)
	–1 Si 307.1(2)	–1 Pd 335.5(1)
	–1 Si 311.9(2)	–1 Ca 346.7(2)
	–1 Pd 312.0(1)	–1 Si 351.6(2)
	–1 Pd 312.1(1)	–2 Ca 373.2(2)
	–1 Si 314.2(2)	–1 Ca 384.9(2)
	–1 Si 316.3(2)	
Si neighbors:		
	–1 Pd 240.8(1)	–1 Ca 307.1(2)
	–1 Pd 242.7(1)	–1 Ca 311.9(2)
	–1 Pd 246.5(1)	–1 Ca 314.2(2)
	–1 Si 271.4(2)	–1 Ca 316.3(2)
	–1 Ca 301.9(2)	–1 Ca 351.6(2)
Pd neighbors:		
	–1 Si 240.8(1)	–1 Ca 312.0(2)
	–1 Si 242.7(1)	–1 Ca 312.1(2)
	–1 Si 246.5(1)	–1 Ca 326.5(2)
	–1 Pd 291.8(1)	–1 Ca 331.0(2)
	–1 Ca 293.1(2)	–1 Ca 335.5(2)
Bond angles:	$Pd^{Si}Pd$ 119.7(1)	$Si^{Pd}Si$ 133.2(1)
	90.4(1)	117.8(1)
	73.2(1)	106.8(1)

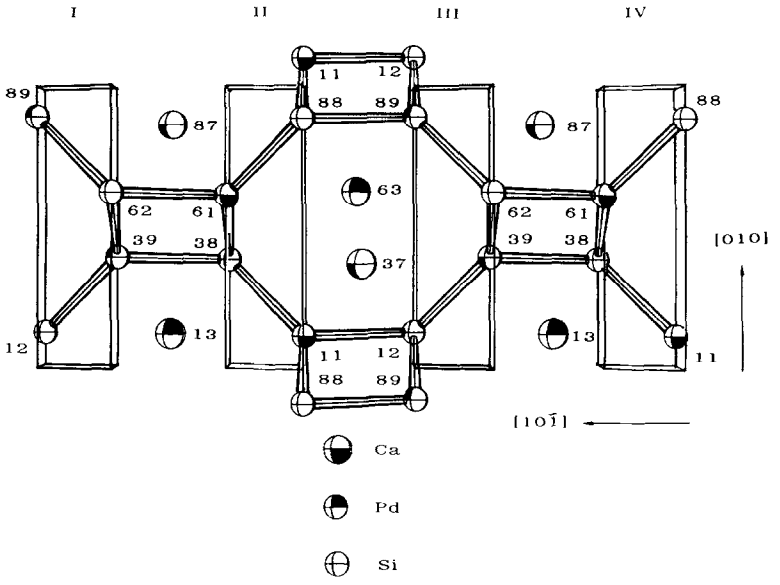

FIG. 5. Building up a 4.8^2 motif by connection of screws of three-connected Pd and Si atoms with different chirality at nearly the same height *y* (presented as multiples 1/100). The screws numbered from I to IV correspond to those shown in Fig. 4b. Two Ca atoms lie above and below one octagon of the distorted 4.8^2 net (compare Fig. 3b).

distorted 4.8^2-nets are shifted in the $(10\bar{1})$ plane so that the layer sequence A,B,A is changed to A,B,C,A . . . (Fig. 4b). The layers of three-connected Pd and Si atoms are separated by Ca atoms with two of them always lying above and below the distorted octagons in the 4.8^2-net (Fig. 5). In the LaIrSi-type structure two metal atoms also fill one cavity formed by three-connected *T* and *S* atoms, but this cavity projects only as an octagon (Fig. 3b). Nevertheless, in the LaIrSi and in the CaPdSi type structure the *M* atoms are placed symmetrically to the bond between the screws. Surprisingly, the heights of the *M* atoms—presented as multiples of 1/100—are equal for SrPdSi and CaPdSi: 13, 37, 63, 87 (Figs. 3b, 4b). However, in CaPdSi each Ca atom has four Ca neighbors in the range 346.7(2) to 384.9(2) pm (Table VIII), in CaPtSi I with the LaIrSi-type structure each Ca atom has six Ca neighbors up to 387.1(3) pm (*1*). Also, the number of *T* and *S* neighbors is lower in CaPdSi than in CaPtSi I, but their distance is smaller in the first: Ca has six Pd neighbors in the range 293.1(1) to 335.5(1) pm (Table VIII) and six Si neighbors in the range 301.9(2) to 351.6(2) pm. In the second the Ca atoms have seven Pt neighbors in the range 316.9(6) to 370.8(7) pm and seven Si neighbors in the range 320.8(11) to 365.0(13) pm (*1*). Bond distances and bond angles within one 4.8^2-motif in CaPtSi I and in CaPdSi are presented in Fig. 6.

In CaPdSi the distances Ca–Ca, Ca–T, and Ca–S are slightly decreased in comparison to CaPtSi I, but the opposite is true for the T–S distances. In CaPdSi each Pd atom has three Si neighbors at 240.8(1), 242.7(1), and 246.5(1) pm (and vice versa) (Table VIII). The averaged Pd–Si distance of 243 pm in CaPdSi is about 13 pm longer than the Pt–Si distance in CaPtSi I with the LaIrSi-type structure (229.7(5) pm) (*1*), although the metallic radius of Pt is slightly higher than that of Pd. It seems that this is a conse-

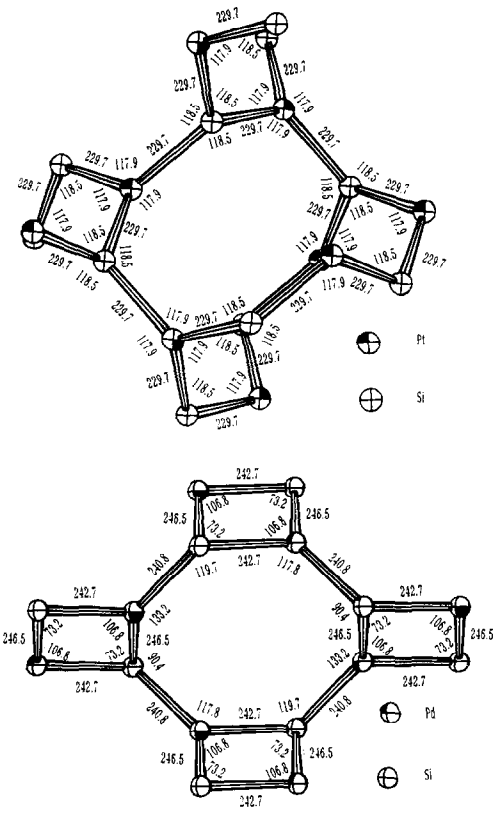

FIG. 6. Bond distances and bond angles within one 4.8^2 motif: (a) in the distorted 3D3C-net of CaPtSi I [1] and (b) in a layer in CaPdSi.

quence of the increased space filling of CaPdSi in comparison to CaPtSi: it is well-known that bond distances become larger with denser packing and increasing coordination number.

By inspection of Table VIII it is seen that the three-connected Si atoms have also one Si neighbor at 271.4(2) pm and the three-connected Pd atoms one Pd neighbor at 291.8(1) pm. However, the Pauling bond order for these distances is low (0.4, 0.2, respectively), but it shows a trend for increasing coordination numbers of the Si and the Pd atoms in CaPdSi from 3 to 4. It is interesting that at 4 GPa and 1100°C the EuNiGe-type structure of CaPtSi II can be transformed into a denser packed one. The Guinier powder diffractogram of the third polymorph of CaPtSi is indexable with the orthorhombic lattice of the TiNiSi-type structure (*26, 27*). Here each T atom has four Si neighbors (and vice versa).

It seems that the EuNiGe-type structure is a hitherto missing link between the LaIrSi-type structure with a three-connected and the TiNiSi-type structure with a four-connected net.

Acknowledgments

Thanks are due to the Fonds der Chemischen Industrie.

References

1. J. EVERS AND G. OEHLINGER, *J. Solid State Chem.* **62,** 133 (1986).
2. K. KLEPP AND E. PARTHÉ, *Acta Crystallogr Sect. B* **38,** 1541 (1982).
3. A. F. WELLS, *Acta Crystallogr.* **7,** 535 (1954).
4. A. F. WELLS, *Acta Crystallogr.* **9,** 23 (1956).
5. A. F. WELLS, *Acta Crystallogr.* **16,** 857 (1963).
6. A. F. WELLS, *Acta Crystallogr Sect. B* **28,** 711 (1972).
7. A. F. WELLS, "Structural Inorganic Chemistry," 5th ed., p. 110, Clarendon Press, Oxford (1984).
8. A. F. WELLS, "THREE-DIMENSIONAL NETS AND POLYHEDRA," WILEY, NEW YORK (1977).
9. A. F. WELLS, *J. Solid State Chem.* **54,** 378 (1984).
10. K. H. JANZON, H. SCHÄFER, AND A. WEISS, *Angew, Chem.* **77,** 258 (1965).
11. J. EVERS, *J. Solid State Chem.* **24,** 199 (1978).
12. J. EVERS, Habilitationsschrift, Universität München 1982.
13. J. EVERS, G. OEHLINGER, AND A. WEISS, *Angew. Chem.* **90,** 562 (1978).
14. J. EVERS, *J. Solid State Chem.* **77,** 32 (1980).
15. C. ZHENG AND R. HOFFMANN, *Inorg. Chem.* **28,** 1074 (1989).
16. D. LOUER AND R. VARGAS, *J. Appl. Crystallogr.* **15,** 542 (1982).
17. W. B. PEARSON, "The Crystal Chemistry and Physics of Metals and Alloys," Wiley–Interscience, New York/London/Sydney/Toronto (1972).
18. D. B. WILES AND R. A. YOUNG, *J. Appl. Crystallogr.* **14,** 149 (1981).
19. B. SENDLINGER, Diplomarbeit, Universität München (1989).
20. J. EVERS, G. OEHLINGER, C. PROBST,

M. SCHMIDT, P. SCHRAMEL, AND A. WEISS, *J. Less-Common Met.* **81,** 15 (1981).

21. P. SCHRAMEL, unpublished results.
22. K. SAGEL, Tabellen zur Röntgenstuikturanalyse, Springer Verlag, Berlin (1958).
23. G. SHELDRICK, "SHELXTL, Program for the Solution of Crystal Structures" University of Göttingen, D-3400 Göttingen, FRG.
24. B. D. ONISKOVETS, V. K. BELSKII, V. K. PECHARSKI, AND O. I. BODAK, *Kristallografiya* **32,** 888 (1987). [*Soviet Phys. Crystallogr.* **32,** 522 (1987)].
25. G. S. SMITH AND R. L. SNYDER, *J. Appl. Crystallogr.* **12,** 60 (1979).
26. C. B. SHOEMAKER AND D. P. SHOEMAKER, *Acta Crystallogr.* **18,** 900 (1965).
27. E. HOVESTREYDT, N. ENGEL, K. KLEPP AND E. PARTHE', *J. Less-Common Met.* **85** 247 (1982).